

Pulse-Width Modulation Pre-Emphasis Applied in a Wireline Transmitter, Achieving 33 dB Loss Compensation at 5-Gb/s in 0.13- μ m CMOS

Jan-Rutger (J. H. R.) Schrader, *Student Member, IEEE*, Eric A. M. Klumperink, *Member, IEEE*, Jan L. Visschers, *Member, IEEE*, and Bram Nauta, *Senior Member, IEEE*

Abstract—A transmitter pre-emphasis technique for copper cable equalization is presented that is based on pulse-width modulation (PWM). This technique is an alternative to the usual 2-tap symbol-spaced FIR (SSF) pre-emphasis. The technique uses timing resolution instead of amplitude resolution to adjust the filter transfer function, and therefore fits well with future high-speed low-voltage CMOS processes. Spectral analysis and time domain simulations illustrate that PWM pre-emphasis offers more relative high frequency boost than 2-tap SSF. Only one coefficient needs to be set to fit the equalizer transfer function to the channel, which makes convergence of an algorithm for automatic adaptation straightforward. A proof-of-concept 0.13- μ m CMOS transmitter achieves in excess of 5 Gb/s (2-PAM) over 25 m of standard RG-58U low-end coaxial copper cable with 33 dB of channel loss at the Nyquist frequency (2.5 GHz). Measured BER at this speed and channel loss is $< 10^{-12}$.

Index Terms—CMOS integrated circuits, copper, equalizers, pulse-width modulation, transceivers, transmit pre-emphasis, transmit pre-shaping, wire communication.

I. INTRODUCTION

IN HIGH-SPEED data communication over copper cables, skin-effect and dielectric losses cause inter-symbol interference (ISI), decreasing the eye opening and thus limiting the bit rate at which data can still be reliably detected at the receiver side. A good approximation for the cable frequency transfer function $H_c(f)$ (excluding propagation delay) is given by [1], [2]

$$H_c(f) = e^{-\sqrt{j2\pi f\tau_1} - 2\pi f\tau_2}. \quad (1)$$

The skin effect (time constant τ_1) and the dielectric loss (time constant τ_2) cause dispersion and frequency dependent attenuation. The time constants are dependent on cable properties like length, conductance, dielectric permittivity etc. As an example, Fig. 1 shows the simulated response of a 25-m RG-58U coaxial cable to a 5-Gb/s 2-PAM signal. The simulation model, which includes both skin-effect and dielectric losses, is explained later. Clearly, this response is severely distorted by ISI.

Manuscript received September 5, 2005; revised December 19, 2005. This work was supported by Stichting FOM.

J. H. R. Schrader, E. A. M. Klumperink, and B. Nauta are with the CTIT Research Institute, IC Design Group, University of Twente, 7500AE Enschede, The Netherlands (e-mail: j.h.r.schrader@utwente.nl).

J. L. Visschers is with the National Institute for Nuclear Physics and High Energy Physics (NIKHEF), 1098SJ Amsterdam, The Netherlands.

Digital Object Identifier 10.1109/JSSC.2006.870897

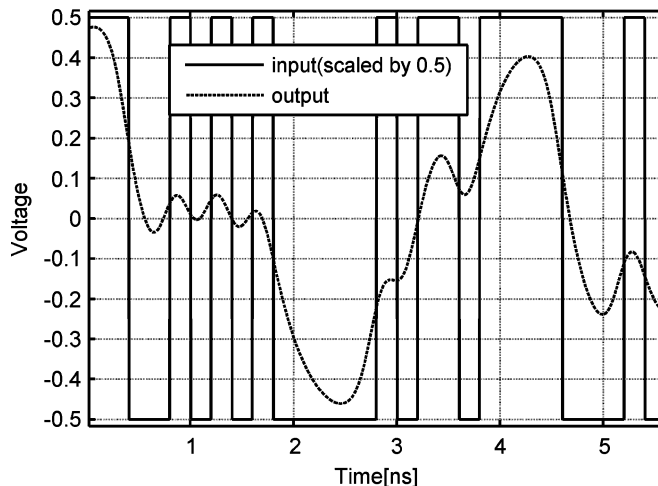


Fig. 1. Simulated response of 25-m RG-58U coaxial cable to 5-Gb/s data.

To compensate for channel losses, transmitter pre-emphasis and receiver equalization are generally applied [3]–[6]. Receiver equalization typically involves several analog blocks which impose speed, accuracy and noise requirements. However, transmitter pre-emphasis allows the use of a simple receiver that only needs to sample binary values [4]. Pre-emphasis methods commonly found in the literature are based on symbol-spaced finite impulse response (SSF) filtering [3]–[6].

This paper presents pulse-width modulation pre-emphasis (PWM-PE) as an alternative to FIR pre-emphasis. A similar technique was shown by the authors' group to perform well for RC limited on-chip wires [7]. However, on quite another channel, copper cables for board-to-board interconnects, the PWM-PE technique also offers a very high level of loss compensation. This was already shown experimentally by the authors in [8]. In this paper, PWM-PE for copper cable interconnects is analyzed in depth and compared to the commonly used 2-tap SSF. Many properties of the PWM-PE filter are similar to those of 2-tap SSF: both have a straightforward implementation, and both are single-coefficient filters, making a coefficient finding algorithm converge more straightforwardly than for multiple coefficients. In comparison to 2-tap SSF, the PWM scheme has a higher switching frequency. The spectral analysis presented in this paper shows that it achieves more high-frequency boost than 2-tap SSFs, resulting in better loss compensation for copper cables. Whereas FIR tunes the pulse amplitude (tap weights) to adjust the filter characteristic to the cable, the PWM-PE filter instead exploits timing resolution and

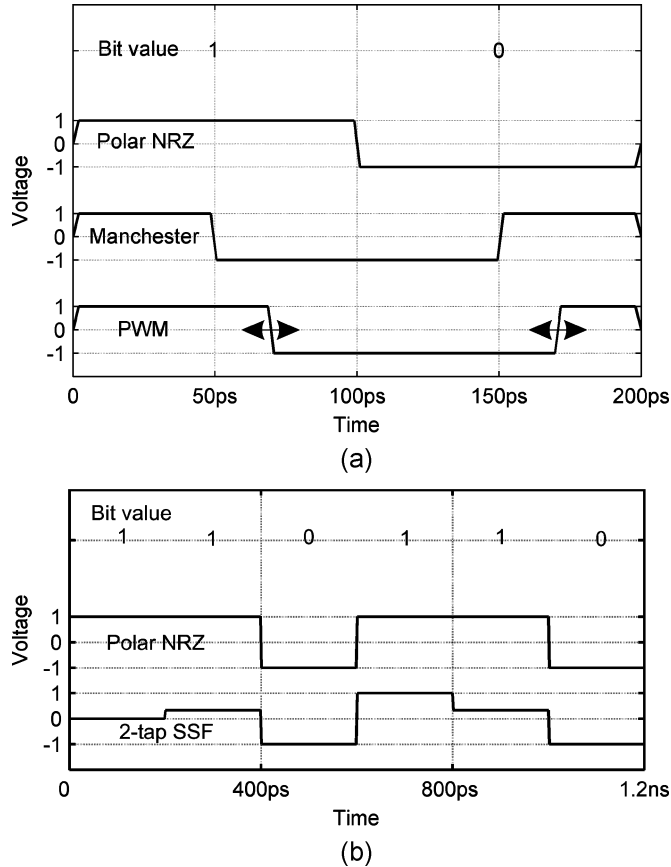


Fig. 2. (a) TX signal for PWM-PE, $T_s = 200$ ps. (b) TX signal for 2-tap SSF-PE, $T_s = 200$ ps.

does not adjust amplitudes. This will be beneficial in future CMOS generations, because of ever-increasing switching speeds, whereas voltage headroom is becoming lower. The filter can be implemented with a low area and a low power consumption because it involves only an adjustable duty-cycle.

The contents of this paper are as follows. Section II gives a first-order time domain insight, then analyzes the frequency transfer of the PWM-PE filter and finally compares it to that of 2-tap SSF pre-emphasis. In Section III, numerical simulations are presented that further explore the properties of the PWM-PE filter in the time domain, showing that ISI can be suppressed better by the PWM-PE filter than by the 2-tap SSF. In Section IV, the prototype circuit is presented. Section V describes the measured performance of the circuit. Finally, conclusions are drawn in Section VI.

II. ANALYSIS OF PRE-EMPHASIS FILTERS

A. Pulse-Width Modulation Pre-Emphasis

In Fig. 2(a), the output voltage waveform for the presented PWM-PE filter is shown. The PWM pulse shape resembles a Manchester-coded signal, but where the Manchester duty-cycle is fixed at 50%, the PWM signal instead has a tunable duty-cycle. A duty-cycle of 100% corresponds to transmission of a normal polar NRZ data signal without pre-emphasis, and 50% to transmission of a Manchester coded data signal (maximum pre-emphasis setting). The optimum duty-cycle is somewhere in between, depending on the channel characteristics.

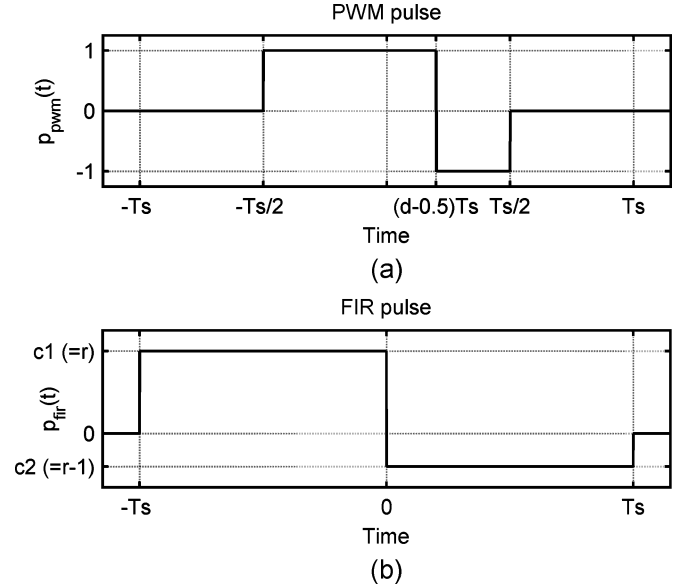


Fig. 3. (a) Definition of pulse shape of PWM-PE. (b) Definition of pulse shape of 2-tap SSF-PE.

An exact definition of the PWM-PE TX signal is given now. First the transmitted data pattern $data_{tr}(t)$ is defined as

$$data_{tr}(t) = \sum_{n=-\infty}^{\infty} u_n p(t - nT_s) \quad (2)$$

where $u_n \in \{-1, 1\}$ denotes the random data, T_s is the symbol duration, and $p(t)$ is the pulse shape. The PWM pulse $p(t) = p_{pwm}(t)$ is defined as follows [illustration in Fig. 3(a)]:

$$p_{pwm}(t) = \begin{cases} 0, & t < -T_s/2 \\ 1, & -T_s/2 \leq t < (d - 0.5) \cdot T_s \\ -1, & (d - 0.5) \cdot T_s \leq t < T_s/2 \\ 0, & T_s/2 \leq t \end{cases} \quad (3)$$

where d denotes the duty-cycle ($0.5 < d < 1$ fits best to copper cables) and T_s denotes the symbol duration. For a quick insight into PWM-PE filtering, the simulated time domain response of a 25-m low-cost, low-end, standard RG-58U cable to PWM pulses with several duty-cycles and $T_s = 200$ ps is shown in Fig. 4. This cable is used later in the experiments. The cable model includes both skin-effect and dielectric losses, and is explained later. The sample moment t_s is shown with a triangle, and the ISI contributions are shown with circles. Note that for the duty-cycle setting of 55%, the cable output pulse becomes much narrower than the response to a plain polar NRZ pulse (100%). This reduces the ISI contributions significantly. It is seen that an optimum setting can be found at which the ISI is minimized. Second, note that the optimum duty-cycle is near—but not equal to—50%. As a comparison, in Fig. 5 the response of the channel to 2-tap SSF pulses is shown. It can be seen that PWM-PE is capable of narrowing the channel pulse response, similar to FIR pre-emphasis. A more detailed comparison between the two techniques is given shortly.

In practice, PWM duty-cycle d can be adapted to the channel automatically using return channel communication and a control algorithm. The need for a return channel is a disadvantage compared to receiver equalization, but it is common among all

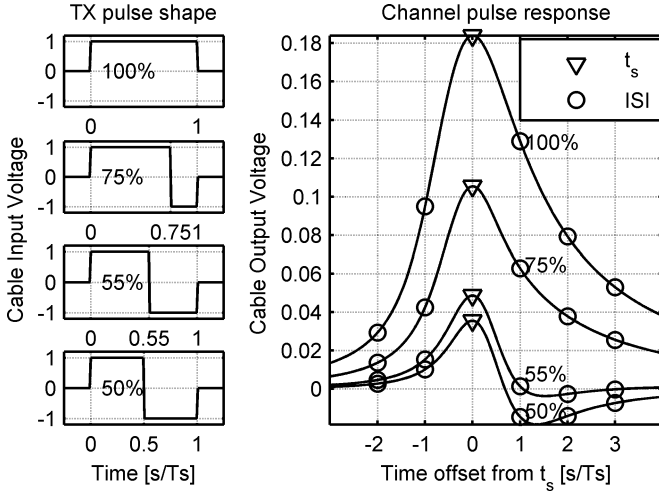


Fig. 4. TX pulse shapes ($T_s = 200$ ps) of PWM-PE filter with varying duty-cycles and simulated responses of 25-m RG-58U cable.

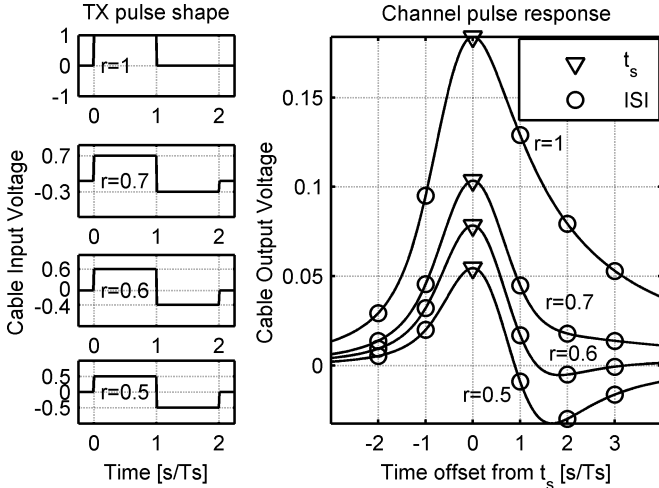


Fig. 5. TX pulse shapes ($T_s = 200$ ps) of SSF-PE filter with varying r parameter and simulated responses of 25-m RG-58U cable.

pre-emphasis approaches. A sign-sign block least mean squares (LMS) algorithm can be used as shown in [9]. Such a control algorithm could also compensate for temperature and channel variations. Convergence of the LMS algorithm for the single-coefficient PWM-PE filter is more straightforward than it would be for a filter with multiple coefficients.

The frequency domain transfer function of the PWM-PE filter is now compared to that of the 2-tap SSF. The TX output swing is normalized to ± 1 V. The spectrum $P_{\text{pwm}}(f)$ of the PWM pulse is calculated by taking the Fourier transform of $p_{\text{pwm}}(t)$:

$$\begin{aligned}
 P_{\text{pwm}}(f) &= \int_{-\infty}^{\infty} p_{\text{pwm}}(t) e^{-j2\pi ft} dt \\
 &= \int_{(d-0.5)T_s}^{(d-0.5)T_s + T_s} e^{-j2\pi ft} dt \\
 &\quad + \int_{(d-0.5)T_s}^{(d-0.5)T_s} -e^{-j2\pi ft} dt. \quad (4)
 \end{aligned}$$

Simplifying leads to

$$P_{\text{pwm}}(f) = \frac{2}{j\omega} \left(\cos\left(\frac{2\pi f T_s}{2}\right) - e^{-j2\pi f(d-0.5)T_s} \right). \quad (5)$$

Next, the transfer function $H_{\text{pwm}}(f)$ of the PWM-PE filter is calculated as follows:

$$H_{\text{pwm}}(f) = \frac{P_{\text{pwm}}(f)}{P_{\text{NRZ}}(f)} \quad (6)$$

where $P_{\text{NRZ}}(f)$ is the spectrum of a normal polar NRZ pulse of width T_s and height 1, which is well known to be

$$P_{\text{NRZ}}(f) = \frac{1}{\pi f} \sin\left(\frac{2\pi f T_s}{2}\right). \quad (7)$$

The expression for $H_{\text{pwm}}(f)$ now becomes

$$H_{\text{pwm}}(f) = \frac{\cos\left(\frac{2\pi f T_s}{2}\right) - e^{-j2\pi f(d-0.5)T_s}}{j \sin\left(\frac{2\pi f T_s}{2}\right)}. \quad (8)$$

Taking the modulus yields

$$\begin{aligned}
 |H_{\text{pwm}}(f)| &= \frac{\sqrt{\cos^2\left(\frac{2\pi f T_s}{2}\right) - 2 \cos\left(\frac{2\pi f T_s}{2}\right) \cos(2\pi f(d-0.5)T_s) + 1}}{\sin\left(\frac{2\pi f T_s}{2}\right)}. \quad (9)
 \end{aligned}$$

This function is illustrated in Fig. 6(a) for several values of d . It can be seen from this figure that a duty-cycle closer to 50% results in a steeper transfer function. This is caused by the fact that changing the duty-cycle from 100% toward 50% attenuates the low-frequency components of the pulse spectrum as compared to the spectrum of a polar NRZ pulse. The result is pre-emphasis filtering. The next section shows how this transfer function compares to that of the 2-tap SSF.

B. 2-Tap Symbol-Spaced FIR (SSF)

In Fig. 2(b), TX waveforms for a 2-tap SSF-PE filter are shown. The 2-tap FIR equalized pulse $p_{\text{fir}}(t)$, shown in Fig. 3(b), is defined as follows:

$$p_{\text{fir}}(t) = \begin{cases} 0, & t < -T_s \\ c_1, & -T_s \leq t < 0 \\ c_2, & 0 \leq t < T_s \\ 0, & T_s \leq t \end{cases} \quad (10)$$

where c_1 and c_2 denote the values of the first and the second FIR taps, respectively, and T_s again denotes the symbol duration. A good fit to copper cables is obtained by choosing $c_1 > 0$ and $c_2 < 0$, while $|c_1| > |c_2|$. The sum of the absolute values of all tap weights has to be limited to the value of the supply to avoid compression at the TX output. When the output swing is again

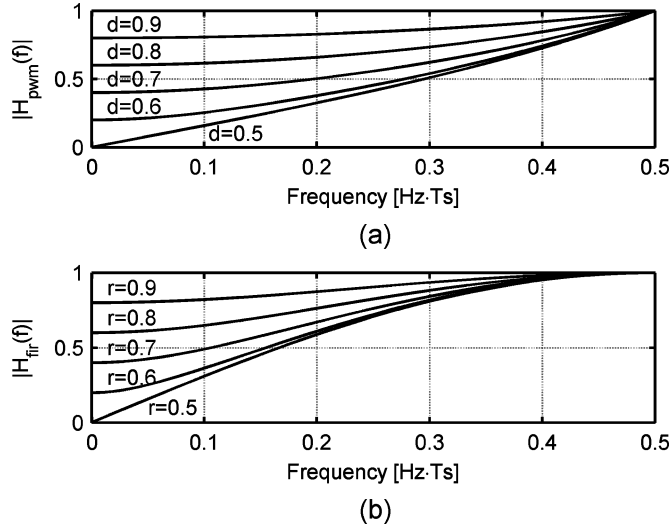


Fig. 6. (a) Calculated normalized magnitude of PWM-PE filter transfer function, for several duty cycles. (b) Calculated normalized magnitude of 2-tap SSF-PE filter transfer function, for several tap weights.

normalized to ± 1 V, as in the previous paragraph, and the whole of the available swing is used, c_1 and c_2 have to comply with

$$|c_1| + |c_2| = 1. \quad (11)$$

These coefficients can be rewritten as $c_1 = r$ and $c_2 = r - 1$ with $r \in \{0.5 \dots 1\}$, resulting in one coefficient r that completely controls the shape of the filter transfer function. Function $p_{\text{fir}}(t)$ now becomes

$$p_{\text{fir}}(t) = \begin{cases} 0, & t < -T_s \\ r, & -T_s \leq t < 0 \\ r - 1, & 0 \leq t < T_s \\ 0, & T_s \leq t \end{cases}. \quad (12)$$

As described before, in practice, this coefficient can be determined automatically using a control loop. Note that for $r = 0.5$ and $T_{s,\text{fir}} = T_{s,\text{pwm}}/2$, the SSF pulse shape is the same as that of a PWM-PE filter with $d = 0.5$. The transfer function $H_{\text{fir}}(f)$ of the 2-tap SSF can be found by using a similar analysis to the one in the previous paragraph, resulting in

$$H_{\text{fir}}(f) = \frac{1}{2} \frac{r e^{j2\pi f T_s} - (r - 1) e^{-j2\pi f T_s} - 1}{j \sin\left(\frac{2\pi f T_s}{2}\right)}. \quad (13)$$

Taking the modulus yields

$$\begin{aligned} & |H_{\text{fir}}(f)| \\ &= \frac{1}{\sqrt{2}} \frac{\sqrt{(1 - \cos(2\pi f T_s)) (2r(r - 1) \cos(2\pi f T_s) + r^2 + (r - 1)^2)}}{\sin\left(\frac{2\pi f T_s}{2}\right)}. \end{aligned} \quad (14)$$

This function is illustrated in Fig. 6(b) for several values of r in the range $\{0.5 \dots 1\}$. It is seen that the closer r is to 0.5, the more low-frequency attenuation the filter exhibits. Comparing it to the PWM transfer in Fig. 6(a), it can be seen that in the

low-frequency (LF) range, the PWM-PE filter behaves like the 2-tap FIR filter, however, in the high-frequency (HF) range, the PWM-PE filter offers a higher loss compensation. Note that both filters leave the amplitude of the fastest data transitions (101010) unchanged, so that the data amplitude at the cable output is exactly the same for both filters.

III. SIMULATION OF ISI REDUCTION

In the previous section, it was shown from a frequency domain perspective that PWM-PE provides more relative HF boost than 2-tap SSF. This section compares the two pre-emphasis methods from a time domain perspective by calculating the remaining ISI at the output of the channel as a function of the bit rate. The goal is to find the maximum achievable bit rate for the pre-emphasis filters at which the remaining ISI is still acceptable. The following approach is used. First, the channel responses to the pre-emphasis pulses $p_{\text{pwm}}(t)$ and $p_{\text{fir}}(t)$ are calculated for a number of bit rates, at the optimum pre-emphasis setting. Next, at these points, the remaining ISI in the received signal is calculated as a function of pre-emphasis setting, symbol length, and channel time constant. The remaining ISI is then plotted and compared between the two different equalizers. Finally, the effect of different channel conditions is analyzed.

A. Cable Model

To calculate time domain channel responses, the impulse responses are used. The inverse Fourier transform is used to derive the cable impulse response $h_c(t)$ from the frequency domain transfer function $H_c(f)$ as given in (1), resulting in

$$h_c(t) = h_1(t) * h_2(t) \quad (15)$$

where $*$ denotes the well known convolution integral, and

$$h_1(t) = \frac{\sqrt{\tau_1}}{2t\sqrt{\pi t}} \cdot e^{-\frac{\tau_1}{4t}} \quad (16)$$

and

$$h_2(t) = \frac{1}{\pi\tau_2} \cdot \frac{1}{1 + (t/\tau_2)^2}. \quad (17)$$

The skin effect is modeled by $h_1(t)$ and the dielectric loss by $h_2(t)$, and time constants are given by τ_1 and τ_2 , respectively. In Fig. 7(a) and (b), $h_1(t)$ and $h_2(t)$ are shown. The x -axes in both plots show time divided by τ_1 and time divided by τ_2 , respectively. The y -axes show $h_1(t) \cdot \tau_1$ and $h_2(t) \cdot \tau_2 \cdot \pi$, respectively. The axes are chosen this way to clearly show the maxima and time span of the functions. It can be seen that $h_1(t)$ is asymmetrical in time with a very long tail, and $h_2(t)$ is symmetrical. Note that these impulse responses are theoretical approximations of the real cable impulse response, but nevertheless accurate enough over the frequency range of interest. A large value for the time constants means that the cable is “slow.” To obtain an indication of the level of ISI at the channel output, the full-width at half-maximum (FWHM) value of the impulse responses can be calculated. The FWHM value of $h_1(t)$ is equal

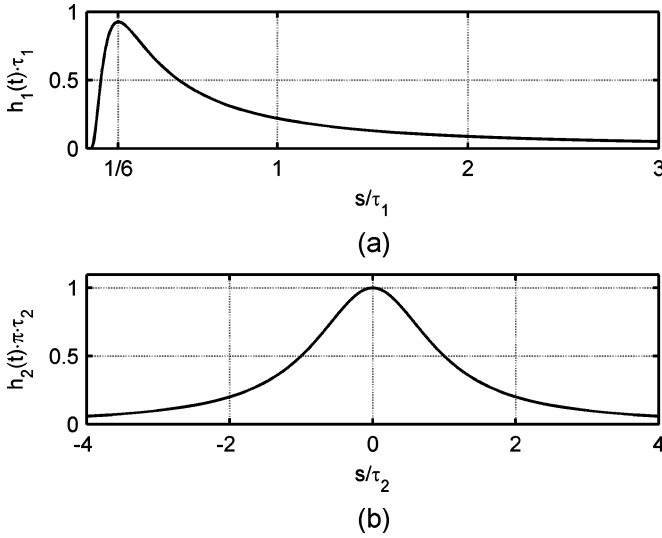


Fig. 7. (a) Theoretical skin-effect impulse response. (b) Theoretical dielectric impulse response.

to approximately $h_{1,\text{FWHM}} = 0.4 \cdot \tau_1$, and the FWHM value of $h_2(t)$ is equal to $h_{2,\text{FWHM}} = 2 \cdot \tau_2$. The RG-58U cable that is used for the measurements at 5 Gb/s, later in this paper, can be modeled with skin-effect time constant $\tau_1 = 0.32$ ns and dielectric time constant $\tau_2 = 0.13$ ns. For this cable, $h_{1,\text{FWHM}} = 0.13$ ns, and $h_{2,\text{FWHM}} = 0.26$ ns.

Two different channel conditions will be analyzed. First, a theoretical channel with only skin loss, and no dielectric loss ($\tau_1 \neq 0, \tau_2 = 0$), is analyzed. The analysis is then repeated for a “dielectric loss only” channel ($\tau_1 = 0, \tau_2 \neq 0$).

B. ISI From Skin-Effect Losses

First, the “skin only” channel will be analyzed. The response $y_{\text{pwm}}(t)$ of the channel to a single PWM pulse is calculated as follows:

$$y_{\text{pwm}}(t) = p_{\text{pwm}}(t) * h_c(t). \quad (18)$$

To quantify the level of remaining ISI, the peak distortion is calculated, which is defined as [10]

$$D_{s_{\text{peak,ISI}}} = \frac{1}{|y_{\text{pwm}}(t_s)|} \sum_{\substack{n=-\infty \\ n \neq 0}}^{n=\infty} |y_{\text{pwm}}(t_s + nT_s)| \quad (19)$$

where t_s is the sample moment. For example, a value of $D_{s_{\text{peak,ISI}}} = 0.2$ means that the eye diagram for the worst case data pattern is 20% closed. In a simple receiver with a bang-bang phase detector, the received signal’s median zero crossing is used for time reference, and then data is sampled at a fixed time, generally $T_s/2$, away from the zero crossing. After that, the ISI contributions can be found at distances of $n \cdot T_s$ from t_s . The peak distortion $D_{s_{\text{peak,ISI}}}$ is a function of the symbol length T_s , the channel time constant τ_1 , the sample moment t_s and the duty-cycle d . A reduction in the number of variables can be made by acknowledging that $D_{s_{\text{peak,ISI}}}$ only depends on the ratio T_s/τ_1 . A large value for T_s/τ_1 means that

the bit rate is very low compared to the channel speed, whereas a small value means the opposite. The expectation is that for very small ratios the ISI becomes unacceptably large, whereas for very large ratios it converges to zero.

The mathematics involved in manipulation of (18) and (19) are rather complicated and do not yield concise symbolic results. Therefore, our resort is numerical computation. In the simulation, the zero-forcing criterion is applied to $D_{s_{\text{peak,ISI}}}$ to find the optimum duty-cycle setting d_{opt} . Then, in Fig. 8(a), the value of $D_{s_{\text{peak,ISI}}}$ at d_{opt} is plotted versus T_s/τ_1 , and in Fig. 8(b) d_{opt} is plotted versus T_s/τ_1 . An identical procedure is followed for the 2-tap SSF PE filter. Again, the minimized $D_{s_{\text{peak,ISI}}}$ for the SSF is plotted in Fig. 8(a), and the optimum SSF coefficient r_{opt} is plotted in Fig. 8(b).¹ Choosing $D_{s_{\text{peak,ISI}}} = 0.2$ for a reasonable eye opening, it can be seen from the figures that the FIR filter reaches this point at $T_s/\tau_1 = 0.19$ whereas the PWM filter reaches it at $T_s/\tau_1 = 0.09$. This means that the PWM-PE achieves twice the bit rate of the 2-tap SSF for the same peak distortion.

Another point of interest is the sensitivity of PWM pre-emphasis to timing errors. An error in the duty-cycle will effectively change the pre-emphasis setting and thus have an effect on the eye opening at the receiver side. However, a certain error can be allowed in the duty-cycle setting. Fig. 8(c) shows the width W_d of the duty-cycle range wherein $D_{s_{\text{peak,ISI}}} < 0.2$. For the 2-tap SSF-PE filter, the same figure shows the width W_r of the range of filter coefficient r wherein $D_{s_{\text{peak,ISI}}} < 0.2$. The y axis in this plot is explained in the following example. From Fig. 8(c) it can be seen that $W_d = 0.057$ at $T_s/\tau_1 = 0.3$, indicated in the figure by a + symbol. From Fig. 8(b), the optimum duty-cycle $d_{\text{opt}} = 0.565$ indicates the middle of this range. This means that a duty-cycle in the range $\{0.537, 0.594\}$ will yield a peak distortion $D_{s_{\text{peak,ISI}}} < 0.2$. Next, for 2-tap SSF, from Fig. 8(c), $W_r = 0.054$ at $T_s/\tau_1 = 0.3$, indicated in the figure by a circle. From Fig. 8(b), the optimum r parameter $r_{\text{opt}} = 0.610$ indicates the middle of this range. This means that a value for r in the range $\{0.583, 0.637\}$ will yield a peak distortion $D_{s_{\text{peak,ISI}}} < 0.2$. It can be seen that both W_d and W_r become smaller with increasing bit rate. The identical behavior in Fig. 8(c) illustrates the interchangeability of timing and amplitude precision.

C. ISI From Dielectric Losses

As in the previous paragraph, the simulations can be run for the second channel, which exhibits only dielectric loss ($\tau_1 = 0, \tau_2 \neq 0$). The value of $D_{s_{\text{peak,ISI}}}$ is plotted as a function of T_s/τ_2 in Fig. 9(a) for both the 2-tap SSF and the PWM-PE filter. In Fig. 9(b), d_{opt} is plotted versus T_s/τ_2 ($\tau_1 = 0$). Note that the time axis is much longer than in Fig. 8, although it has to be taken into account that $h_{2,\text{FWHM}}$ divided by τ_2 is approximately five times larger than $h_{1,\text{FWHM}}$ divided by τ_1 . Comparing Fig. 9(a) to Fig. 8(a), the performance of both filters on channels dominated by dielectric loss is expected to be worse than for channels dominated by skin-effect. This is related to

¹Several different regions can be identified in the plots. In each region, another ISI term dominates the response (pre-cursor, first post-cursor, second post-cursor, etc.).

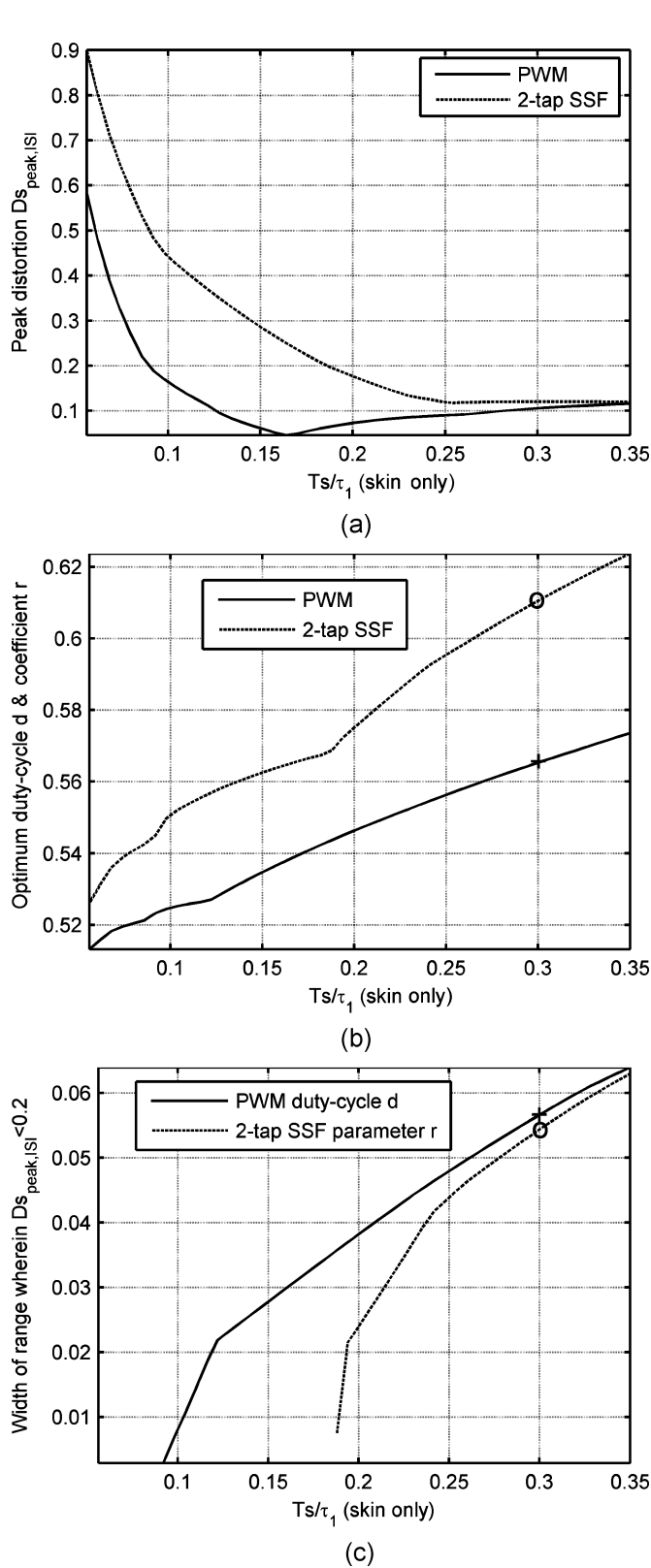


Fig. 8. (a) Simulated minimized peak distortion for skin channel. (b) Simulated optimum PWM duty-cycle and FIR coefficient for skin channel. (c) Simulated range width for $D_{s_{peak,ISI}} < 0.2$ of d (PWM) and r (2-tap SSF).

the difference in symmetry between the skin-effect impulse response and the dielectric impulse response.

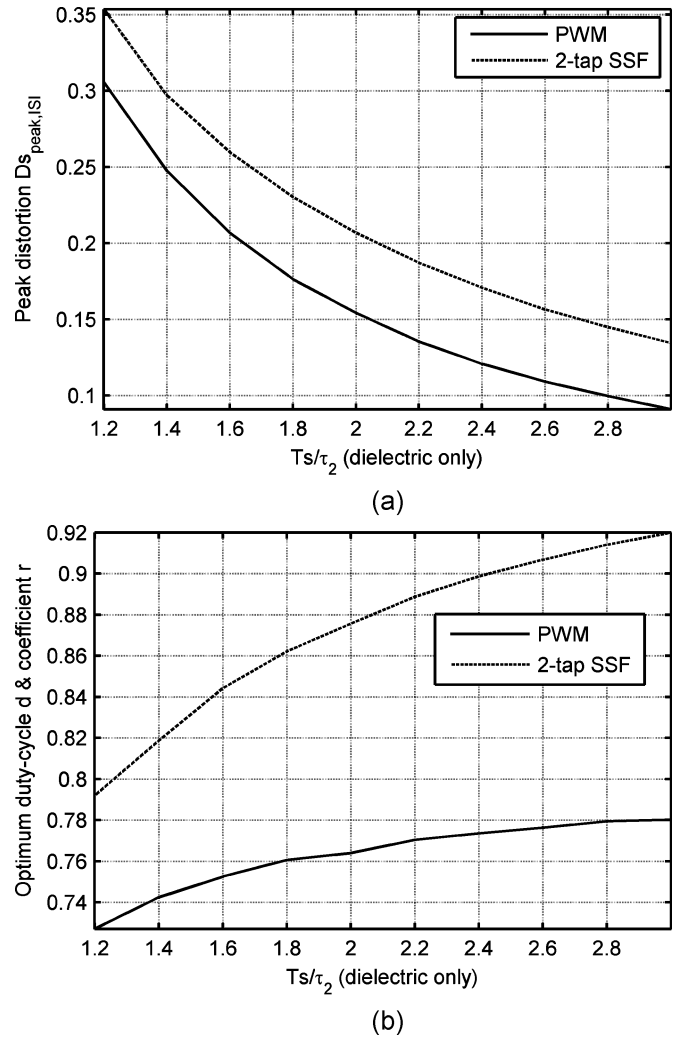


Fig. 9. (a) Simulated minimized peak distortion for dielectric channel. (b) Simulated optimum PWM duty-cycle and FIR coefficient for dielectric channel.

Finally, an estimation of the performance of the PWM-PE filter in the upcoming measurements is made by using the simulation results above. The 25-m-long RG-58U cable is used at a bit rate of 5 Gb/s, which corresponds to $T_s/\tau_1 = 0.63$ and $T_s/\tau_2 = 1.54$. The value of 0.63 is not on the x axis of Fig. 8(a) and can be assumed to correspond to a low level of remaining ISI. However, the value of 1.54 corresponds to $D_{s_{peak,ISI}} = 0.22$ in Fig. 9(a), which indicates that the dielectric loss will limit the achievable bit rate for this cable.

IV. CIRCUIT IMPLEMENTATION

A prototype circuit is designed as a proof-of-concept. As shown in Fig. 10(a), the data is XORed with a pulse-width modulated clock in order to provide pre-emphasized data. The PWM clock is generated using an OR gate and a delay circuit. The timing of the signals is illustrated in Fig. 10(b). Fig. 11 shows the chip diagram. Because a small differential delay is more straightforward to generate than a short absolute delay, the relative delay for clock B is created by delaying $clk1$ with delay1 and delaying $clk2$ with delay2. The differential delay is thus equal to (delay1-delay2) and is controllable by voltage $V_{delay1} - V_{delay2}$. Both are differential voltages. The XOR is

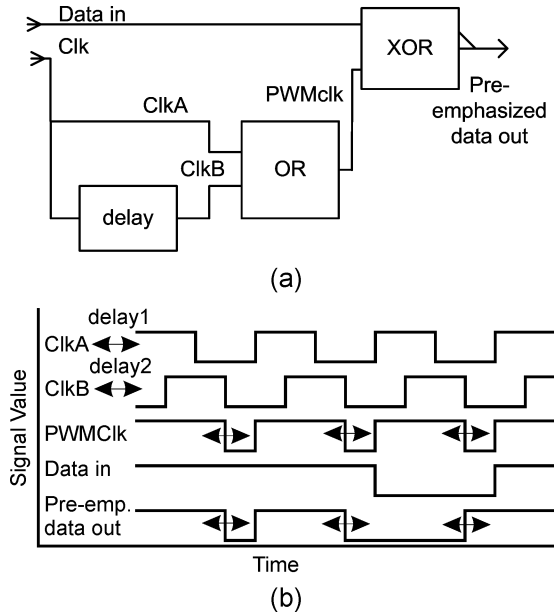


Fig. 10. (a) Circuit operation principle. (b) Signals used in generating PWM signal.

implemented using a multiplexer [Fig. 12(a)] that selects either noninverted data $D1$ or inverted data $D2$. For an optimum timing margin, $D2$ is delayed by half a symbol time using a negative edge clocked flip-flop [7]. The duty-cycle of the PWM pulse shape can be tuned between 50%–100%, provided the relative phase-shift between clocks is adjustable from 0° to 180° .

The whole test chip is designed in current-mode logic (CML) to provide maximum supply noise rejection and minimum supply noise injection and to keep timing noise as low as possible. As with FIR pre-emphasis, any bandwidth limitations in the circuitry will just become part of the total channel transfer function that needs to be compensated by the pre-emphasis. An advantage over FIR pre-emphasis is that nonlinear slewing effects do not affect the equalizer's fit to the channel because only two signal levels are used. The duty-cycle can be adjusted to compensate for changes in the transfer function. A difference between up and down slew rate would have a negative effect on the fit of the pre-emphasis to the channel. The use of differential CML guarantees equal up and down slew rates.

A. Delay Circuit

The time-shifted clock is generated using a variable delay circuit [Fig. 12(b)] [11]. The delay between input and output of this circuit is mainly determined by the RC time at the output. By adding a positive feedback circuit in parallel to the output, which effectively behaves as a negative resistance, the effective R can be changed and hence the RC-delay is changed. The value of the negative resistance is controlled by the differential delay control voltage $V_{\text{delay}} (= V_{\text{delP}} - V_{\text{delN}})$, which divides the total bias current between the input differential pair and the negative resistance pair. For $V_{\text{delP}} \gg V_{\text{delN}}$, the delay is minimized. As the total bias current through the output resistors is fixed, the output swing remains constant. The required tuning range of the delay

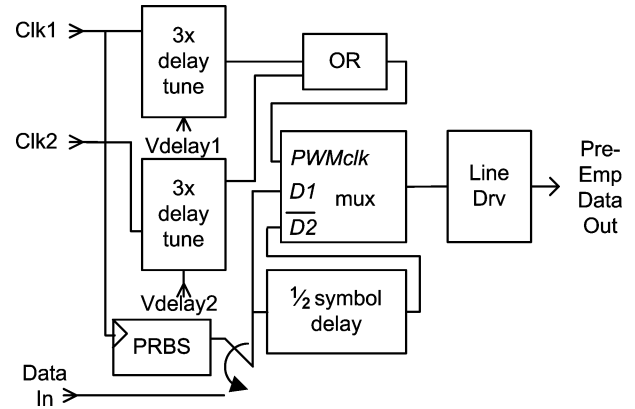


Fig. 11. Chip diagram: PRBS generator, pre-emphasis circuit, and line driver.

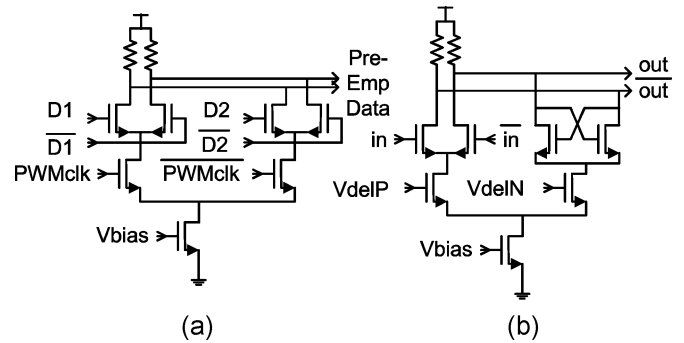


Fig. 12. (a) CML multiplexer. (b) CML delay tuning circuit.

circuit depends on the desired symbol length and on the necessary duty-cycle range for pre-emphasis. The continuous tuning range can be enlarged by cascading multiple delay stages. For very large delay ranges, this becomes impractical and it is more effective to combine the continuously tunable delay with discrete fixed delay steps. The prototype design is designed to give the flexibility needed to evaluate the new PWM-concept in various ways. Therefore, external clocks can be provided, for example to accommodate very low bit rates for long, poor cables. During normal operation, both inputs $clk1$ and $clk2$ (Fig. 11) can just be connected to the same clock.

B. Line Driver

The line driver (Fig. 13) consists of three stages. Each stage has three times the W/L dimensions and one-third the resistance value of its predecessor. The final stage has $50\text{-}\Omega$ on-chip output resistance and a tail current of 24 mA. The nominal single-ended output swing is $600\text{ mV}_{\text{pp}}$, which corresponds to a differential voltage of 1.2 V_{pp} .

V. MEASUREMENTS

A microphotograph of the chip is shown in Fig. 14. The chip measures $1 \times 1\text{ mm}^2$. To evaluate the performance of the prototype chip, a number of measurements are made. First, eye diagrams are generated, to provide a first-order estimation of the signal integrity and to see the effect of adjusting the duty-cycle setting. Second, BER measurements are made using an external pattern generator and BER tester to evaluate the robustness and reliability of the transmitter. All measurements are made using

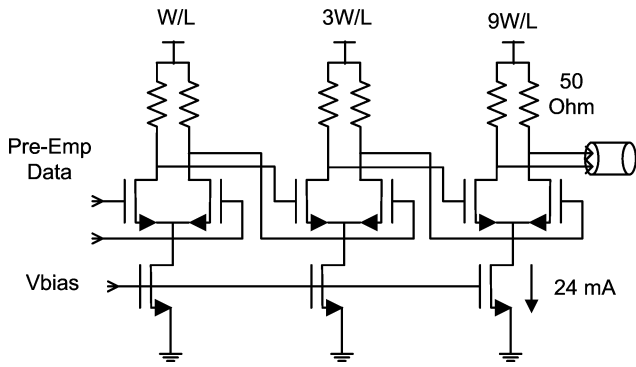


Fig. 13. Three-stage differential line driver.

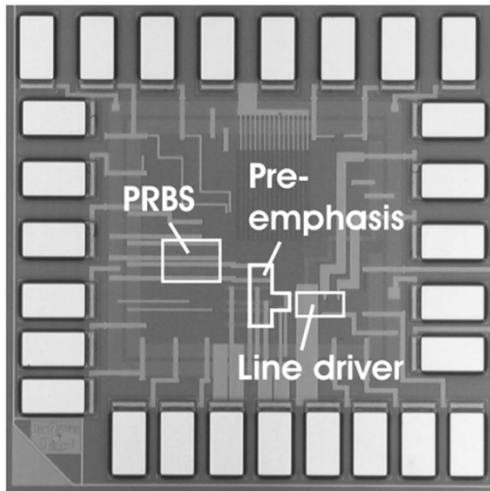


Fig. 14. Chip microphotograph, 1 × 1 mm².

standard RG-58U coaxial cable, using only one of the two transmitter outputs and terminating the other with a 50-Ω dummy. The cable is connected to the test chip using a 50-Ω differential probe with four pins: ground-signal-signal-ground. All chip I/Os have on-chip 50-Ω termination and are ESD protected. If the chip is mounted on a PCB, there might be an impedance change from the PCB to the cable, causing reflections. These reflections will be largely absorbed by the transmitter termination resistors. PWM-PE alone is unable to compensate for a channel with reflections, because it offers only one degree of freedom. However, this problem is also present when using 2-tap SSF pre-emphasis. A possible solution is the use of a receiver equalizer that cancels reflections. The requirements for such an equalizer can be relatively low compared to the case with no TX pre-emphasis, as the largest part of the necessary loss compensation will be generated at the TX side.

A. Effect of Adjustments in PWM Duty-Cycle

In Fig. 15, the effect of adjusting the PWM duty-cycle on the transmitter output can be seen. The TX output eyes are shown for different duty-cycles. The left- and right edges in the eye diagrams correspond to the symbol edges. In Fig. 16, the responses of a 10-m RG-58U cable to the pre-emphasized data stream with different pre-emphasis duty-cycles are shown. It can be seen that

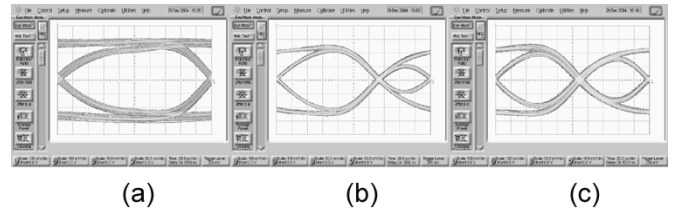


Fig. 15. Measured transmitter eyes at 5 Gb/s with three different duty-cycle settings. Horizontal axis = 20 ps/div, vertical axis = 100 mV/div. (a). No pre-emphasis (100%). (b). Optimum pre-emphasis (66%). (c). Strong pre-emphasis (55%).

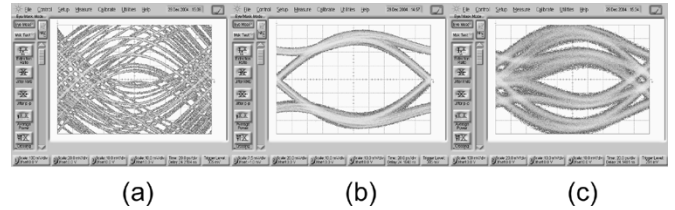


Fig. 16. Measured eyes of cable response for transmitter settings shown in previous figure and 5 Gb/s over 10-m RG-58U cable. Horizontal axis = 20 ps/div, vertical axis = 20 mV/div. (a). No pre-emphasis (100%). (b). Optimum pre-emphasis (66%). (c). Strong pre-emphasis (55%).

there is an optimum duty-cycle [Fig. 16(b)]. Under-emphasis is shown in Fig. 16(a) and over-emphasis in Fig. 16(c). Note that the time scale in Figs. 15 and 16 is the same. The PWM pre-emphasis leaves the fastest data pattern (101010) unchanged while it attenuates the data patterns with less transitions per second.

B. Eye Diagrams at Max. Loss Compensation

In Fig. 17(a) (4 Gb/s) and (b) (5 Gb/s), measured eye diagrams of the cable output for 25-m RG-58U are shown, using an on-chip $2^7 - 1$ PRBS pattern generator. These two speeds are shown to illustrate the difference in eye shape. As shown in Fig. 18, the cable loss at 2.5 GHz is 31 dB, and the total channel loss is approximately 33 dB including additional parasitic losses in the path from chip to coaxial cable, consisting of probes, short wire, bias tee and connectors. Using an external pattern generator and tester, the BER is tested at up to 5 Gb/s and is $< 10^{-12}$.

At a channel loss of 33 dB, the small cable output amplitude imposes a high demand on receiver sensitivity and it might be necessary to use differential signaling. Using the fully differential transmitter capabilities would boost the differential swing at the cable output by 6 dB while also rejecting common mode noise.

In Table I, a comparison with other published work is given. In [5], a combination of pre-emphasis and post-equalization has yielded 27 dB (18 dB + 9 dB) loss compensation at a signaling rate of 5 Gb/s. Here, “loss compensation” is defined as cable loss at the Nyquist frequency, for example, 2.5 GHz for a 5-Gb/s signaling rate, at which low error transmission is still possible. None of the pre-emphasis filters that use two taps [3]–[5] offer more than 18 dB loss compensation. A 5-tap FIR filter in [6] reached 30 dB but only at 3.125 Gb/s. More taps can offer higher loss compensation but at the expense of increasing complexity, possibly causing accuracy and speed problems. Furthermore, algorithm convergence for automatically finding the optimum

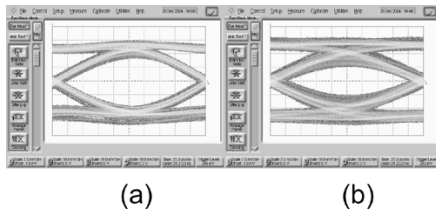


Fig. 17 (a) Measured output eye of 25-m RG-58U at 4 Gb/s. Horizontal axis = 20 ps/div, vertical axis = 10 mV/div. (b) Measured output eye of 25-m RG-58U at 5 Gb/s. Horizontal axis = 20 ps/div, vertical axis = 7.5 mV/div.

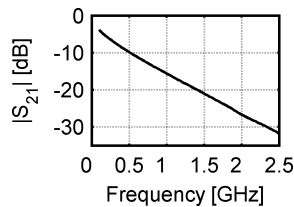


Fig. 18. Measured S_{21} magnitude data for 25-m RG-58U coaxial cable.

TABLE I
PWM PRE-EMPHASIS COMPARISON WITH OTHER WORK

Ref.	R	Loss	Process	Type
[3]	8Gb/s	~10dB	0.3 μ m	2-FIR
[4]	4Gb/s	~10dB	0.25 μ m	2-FIR
[5]	5Gb/s	18dB	0.13 μ m	2-FIR
[6]	3.125Gb/s	30dB	0.11 μ m	5-FIR
this work	5Gb/s	33dB	0.13μm	PWM

equalizer coefficients is more troublesome than for a single-coefficient equalizer. The single-coefficient PWM-PE filter presented here offers the highest loss compensation (33 dB), at a bit rate of 5 Gb/s.

In Table II, the electrical characteristics of the transmitter are given. Power dissipation figures are hard to compare because most publications only give total figures. In the current proof-of-concept design, the clock-buffering takes quite a lot of the power budget, which can be improved when internal clocks are available on the IC. Because of the simplicity of the pre-emphasis method, both the chip area and power consumption can be very small.

VI. CONCLUSION

A new pre-emphasis (PE) technique for copper cable data communication, based on pulse-width modulation (PWM), is introduced. This technique can be used to compensate for cable loss, and is an alternative to symbol-spaced FIR (SSF) pre-emphasis. The PWM method does not tune the pulse amplitude as for FIR pre-emphasis, but instead exploits timing resolution. This fits into the CMOS technology trends toward higher switching speeds and lower voltage headroom. The single-coefficient PWM-PE filter offers a higher relative HF boost than a 2-tap SSF, as shown in theory and by measurements, resulting in higher loss compensation. One important benefit of single-coefficient pre-emphasis, the straightforward automatic finding of the filter coefficient, is retained. A prototype chip is designed, fabricated and measured. The main building blocks of the CML

TABLE II
ELECTRICAL CHARACTERISTICS OF TRANSMITTER

Bit rate (2-PAM)	5Gb/s
U-I	200ps
TX amp. (V_{p-p}) nom.	1.2V (dif), 600mV (s-ended)
Channel loss @ 2.5GHz	33dB
V_{sup}	1.2V
Power (pre-emphasis)	12mW
Power (line driver)	42mW
Power (clock buffering)	39mW
Power (on-chip PRBS)	17mW

pre-emphasis circuit are a tunable delay, an OR gate and a multiplexer. The pre-emphasis technique can be implemented on only a small chip area and with low power consumption. Transmission of a 2-PAM 5-Gb/s data signal over 25 m of low-cost, low-end, standard RG-58U coaxial cable is demonstrated with a BER $< 10^{-12}$. This corresponds to a record loss compensation of 33 dB at the Nyquist frequency of 2.5 GHz.

ACKNOWLEDGMENT

The authors would like to thank Stichting FOM for funding, CERN and G. Cervelli for organizing chip fabrication, D. Schinkel, P. Moreira and H. Verkooijen for helpful discussions, W. C. van Etten for the cable model, M. Kuijk for equipment use, H. de Vries, G. J. M. Wienk, and J. Rövekamp for practical assistance, W. P. Bakker for language correction, and J. W. Schrader for impractical assistance.

REFERENCES

- [1] F. E. Gardiol, *Lossy Transmission Lines*. Norwood, MA: Artech House, 1987.
- [2] P. Grivet and P. W. Hawkes, *The Physics of Transmission Lines at High and Very High Frequencies*. New York: Academic Press, 1970.
- [3] R. Farjad-Rad, C. K. Yang, M. Horowitz, and T. Lee, "A 0.3- μ m CMOS 8 Gb/s 4-PAM serial link transceiver," *IEEE J. Solid-State Circuits*, vol. 35, no. 5, pp. 757–764, May 2000.
- [4] M. Lee, W. Dally, and P. Chiang, "Low-power area-efficient high-speed I/O circuit techniques," *IEEE J. Solid-State Circuits*, vol. 35, no. 11, pp. 1591–1599, Nov. 2000.
- [5] Y. Kudoh, M. Fukaishi, and M. Mizuno, "A 0.13- μ m CMOS 5-Gb/s 10-m 28 AWG cable transceiver with no-feedback-loop continuous-time post-equalizer," *IEEE J. Solid-State Circuits*, vol. 38, no. 5, pp. 741–746, May 2003.
- [6] W. Gai, Y. Hidaka, Y. Koyanagi, J. H. Jiang, H. Osone, and T. Horie, "A 4-channel 3.125 Gb/s/ch CMOS transceiver with 30 dB equalization," in *Symp. VLSI Circuits Dig. Tech. Papers*, Jun. 2004, pp. 138–141.
- [7] D. Schinkel, E. Mensink, E. A. M. Klumperink, A. J. M. van Tuijl, and B. Nauta, "A 3 Gb/s/ch transceiver for RC-limited on-chip interconnects," in *IEEE Int. Solid-State Circuits Conf. (ISSCC) Dig. Tech. Papers*, Feb. 2005, pp. 386–387.
- [8] J. H. R. Schrader, E. A. M. Klumperink, J. L. Visschers, and B. Nauta, "CMOS transmitter using pulse-width modulation pre-emphasis achieving 33 dB loss compensation at 5-Gb/s," in *Symp. VLSI Circuits Dig. Tech. Papers*, Jun. 2005, pp. 388–391.
- [9] J. T. Stonick, G.-Y. Wei, J. L. Sonntag, and D. K. Weinlader, "An adaptive PAM-4 5-Gb/s backplane transceiver in 0.25 μ m CMOS," *IEEE J. Solid-State Circuits*, vol. 38, no. 3, pp. 436–443, Mar. 2003.
- [10] R. W. Lucky, J. Salz, and E. J. Weldon, Jr., *Principles of Data Communication*. New York: McGraw-Hill, 1968.
- [11] B. Razavi, *Design of Analog CMOS Integrated Circuits*. New York: McGraw-Hill, 2001.



Jan-Rutger (J. H. R.) Schrader was born on September 27, 1976, in Enkhuizen, The Netherlands. He received the M.S. degree in electrical and electronics engineering from the University of Twente, Enschede, The Netherlands, in 2001. He is currently working toward the Ph.D. degree in the IC Design Group of the CTIT Research Institute and the Department of Electrical Engineering, Mathematics and Computer Science at the same university.

His research interests include high-speed data communication and mixed-mode CMOS circuits.



Eric A. M. Klumperink (M'98) was born on April 4, 1960, in Lichtenvoorde, The Netherlands. He received the B.Sc. degree from HTS, Enschede, The Netherlands, in 1982. After a short period in industry, he joined the Faculty of Electrical Engineering of the University of Twente in 1984, where he was mainly engaged in analog CMOS circuit design and research. This resulted in several publications and a Ph.D. thesis, in 1997, on the subject of transconductance-based CMOS circuits.

He is currently an Associate Professor at the IC Design Laboratory and also involved in the CTIT Research Institute. He holds four patents and has authored or co-authored more than 50 journal and conference papers. His research interest is in design issues of HF CMOS circuits, especially for front-ends of integrated CMOS transceivers.

Dr. Klumperink is a co-recipient of the ISSCC 2002 Van Vessel Outstanding Paper Award.



Jan L. Visschers was born in 1944, in Winterswijk, The Netherlands. In 1971, he received the Ph.D. degree in theoretical physics from the Free University Amsterdam (VUA).

He was involved in a large variety of projects around several accelerators at NIKHEF, Amsterdam. He participated in the CHORUS neutrino oscillation experiment (WA95) at CERN, Geneva, Switzerland, as a Senior Associate Physicist. He serves as deputy spokesperson for MEDIPIX, a collaboration between 18 universities and research institutes, to

develop photon-counting pixel detectors for X-ray imaging. He now leads a small research and development group at NIKHEF, designing deep-submicron electronic circuits and read-out systems for tiled arrays of pixel chips. He is a member of the Scientific Committee for the International Workshop on Radiation Imaging Detectors. He also serves as a Program Manager for the Eureka project High-Resolution Large Area X-ray Detectors (RELAXD).



Bram Nauta was born in Hengelo, The Netherlands, in 1964. In 1987, he received the M.Sc. degree (*cum laude*) in electrical engineering from the University of Twente, Enschede, The Netherlands. In 1991, he received the Ph.D. degree from the same university on the subject of analog CMOS filters for very high frequencies.

In 1991, he joined the Mixed-Signal Circuits and Systems Department of Philips Research, Eindhoven, The Netherlands, where he worked on high-speed A/D converters. From 1994, he led a research group in the same department, working on analog key modules. In 1998, he returned to the University of Twente, as a full Professor heading the IC Design group which is part of the CTIT Research Institute. His current research interest is high-speed analog CMOS circuits. He is also a part-time consultant in industry, and in 2001, he co-founded Chip Design Works. His Ph.D. thesis was published as the book *Analog CMOS Filters for Very High Frequencies* (Kluwer, 1993). He holds 11 patents in circuit design.

Dr. Nauta received the Shell Study Tour Award for his Ph.D. work. From 1997 to 1999, he served as Associate Editor of the IEEE TRANSACTIONS ON CIRCUITS AND SYSTEMS II, ANALOG AND DIGITAL SIGNAL PROCESSING. In 1998, he served as a Guest Editor and in 2001 became an Associate Editor of the IEEE JOURNAL OF SOLID-STATE CIRCUITS. He is also a member of the technical program committees of ESSCIRC and ISSCC. He was a co-recipient of the ISSCC 2002 Van Vessel Outstanding Paper Award.